Disordered flat phase in a solid-on-solid model of fcc(110) surfaces and dimer states in quantum spin-$\frac{1}{2}$ chains

Giuseppe Santoro
International School for Advanced Studies, Via Beirut 4, 34014 Trieste, Italy

Michele Fabrizio
Institut Laue-Langevin, Avenue des Martyres, Boîte Postale 166X Grenoble France
(Received 22 December 1993)

We present a restricted solid-on-solid Hamiltonian for fcc(110) surfaces. It is the simplest generalization of the exactly solvable body-centered solid-on-solid model which is able to describe a (2×1) missing-row reconstructed surface. We study this model by mapping it onto a quantum spin-$\frac{1}{2}$ chain of the Heisenberg type, with second and third neighbor $S_i^z S_j^z$ couplings. The ground-state phase diagram of the spin-chain model is studied by exact diagonalization of finite chains up to $N = 28$ sites, as well as through analytical techniques. We find four phases in the phase diagram: two ordered phases in which the spins have a Néel type of long-range order (an unreconstructed and a missing-row reconstructed phase, in the surface language), a spin-liquid phase (representing a rough surface), and an intermediate dimer phase which breaks translational invariance and has a doubly degenerate ground state, corresponding to a disordered flat surface. The transition from the (2×1) reconstructed phase to the disordered flat phase belongs to the two-dimensional Ising universality class. A critical (preroughening) line with varying exponents separates the unreconstructed phase from the disordered flat phase. The possible experimental signatures of the disordered flat phase are discussed.

I. INTRODUCTION

Surfaces of fcc metals, in particular (110) faces, display a variety of phase transitions which have been the subject of considerable experimental and theoretical work.

Experimentally, (110) faces of some fcc metals—such as Au or Pt—are reconstructed at low temperature into a (2×1) missing-row structure, whereas other metals—such as Ag, Ni, Cu, etc.—are not. As the temperature is raised, reconstructed surfaces tend to show two separate transitions: a deconstruction transition occurs first, followed, at a higher temperature, by a roughening transition.[1,2] On unreconstructed surfaces, instead, only a roughening transition has been well characterized.[3,4]

On the theoretical side, an interesting and nontrivial interplay has been anticipated between in-plane ordering, related to reconstruction, and vertical ordering, related to roughening.[5] Since then many studies have been devoted to the problem.[6–12]

The situation is somewhat different for the two cases, the unreconstructed and the missing-row reconstructed. For the unreconstructed case, den Nijs has argued that the phase diagram should be qualitatively similar to that of a simple cubic (100) surface.[13] In particular, he proposes that Ag and Pd (which do not reconstruct) are good candidates for the realization of *preroughening*, an additional critical variable-exponent transition from a low temperature ordered phase to an intermediate temperature *disordered flat* phase, previously identified in the context of restricted solid-on-solid models for simple cubic (100) surfaces.[14] The unreconstructed surface possesses a Néel type of order parameter, which characterizes (1×1) order,

$$P_{(1\times1)} = \frac{1}{N}\left\langle \sum_{\mathbf{r}} h_{\mathbf{r}} e^{i\mathbf{G}\cdot\mathbf{r}} \right\rangle . \tag{1}$$

$P_{(1\times1)}$ can take two opposite values at low temperature and vanishes at and above preroughening.[11,15] [Here $h_{\mathbf{r}}$ is the height of each surface atom, N is the number of (1×1) cells of the surface, and $\mathbf{G} = (2\pi/a_x)\hat{\mathbf{x}}$ is the first nonzero reciprocal vector of the lattice, see Fig. 3.)

For the reconstructed case, one has *four* ground states to deal with (instead of the two ground states of an unreconstructed surface), and these can be classified, according to den Nijs,[9] by a clock variable $\theta = 0, \pi/2, \pi, 3\pi/2$, see Fig. 4. The most elementary extended defects which one can consider are *steps*, which change the average height by ±1 and the reconstruction variable by $\Delta\theta = \pi/2$ [*clockwise* or (3×1) steps] or $\Delta\theta = -\pi/2$ [*anticlockwise* or (1×1) steps], and *Ising wall defects* which do not change the average height, and change the reconstruction variable by $\Delta\theta = \pi$.

The interplay between reconstruction and height degrees of freedom makes this situation particularly interesting. The problem has been tackled using two different lines of approach. The first line of approach consists in identifying heuristically the relevant defects which play a role in the problem, and building up models which describe their behavior. In this framework, den Nijs has formulated a *four state clock-step model* on a length scale somewhat larger than the microscopic one.[9] On each cell of a coarse-grained lattice an integer variable $h_{\mathbf{r}}$—representing the average height in the cell—as well

 ©1994 The American Physical Society

as a clock reconstruction variable $\theta_{\mathbf{r}} = 0, \pi/2, \pi, 3\pi/2$ are defined. By assumption, the only actors appearing in the model are Ising wall defects—for which ($\Delta\theta = \pi, \Delta h = 0$)—as well as clockwise ($\Delta\theta = \pi/2, \Delta h = \pm 1$) and anticlockwise ($\Delta\theta = -\pi/2, \Delta h = \pm 1$) steps. den Nijs found that when both types of steps have the same energy—the so-called *zero chirality limit*—the model displays two possible scenarios: (i) if the parameters are such that the energy of an Ising wall E_w is less than roughly twice the energy of a step E_s, by increasing the temperature one goes from a reconstructed phase to a disordered flat phase with an Ising transition, and then to a rough phase with a conventional Kosterlitz-Thouless (KT) transition; (ii) in the other case—$E_w > 2E_s$—the system undergoes a single roughening-induced deconstruction transition.[9] Within the same line of approach, but in the so-called strong chirality limit (only clockwise steps allowed), den Nijs[9] and, independently, Balents and Kardar[10] have tackled the problem by mapping steps into the world lines of one-dimensional (1D) fermions, the Ising wall being represented by a site doubly occupied by a pair of up and down steps. The Hamiltonian describing such a 1D fermion problem is essentially a Hubbard model with an extra term describing dislocations, i.e., the merging of four steps at the boundary of finite terraces on the surface. Scenario (i) above, realized for an attractive Hubbard U, is essentially recovered in this fermion mapping. As for scenario (ii), corresponding to $U > 0$, the roughening-induced deconstruction is now substituted by a doublet of successive phase transitions: first a Pokrovsky-Talapov (PT) transition to a "floating reconstructed" rough phase, and then a further KT transition to a rough disordered phase.[9,10]

While these approaches are interesting *per se*, in that they identify potential scenarios for these surfaces, their outcome is obviously connected to their initial set of assumptions (i.e., identification of the relevant defects, and choice of their mutual interactions).

A more direct line of approach consists in working with solid-on-solid models, which—while still very idealized—are fully microscopic in nature. Kohanoff *et al.*, and, more recently, Mazzeo *et al.*, have introduced a lattice solid-on-solid (SOS) model which is able to deal with both unreconstructed and reconstructed situations.[7,11] Their model is a simple modification of the exactly solvable body-centered solid-on-solid (BCSOS) model[16] obtained by adding a further neighbor interaction, and is quite closely related to the model we will consider here. Using a Monte Carlo simulation Mazzeo *et al.* study two separate points in its phase diagram, intended to describe the case of reconstructed Au(110) and that of unreconstructed Ag(110).[11] For the reconstructed case they confirm a two-transition scenario: an Ising deconstruction transition to a disordered flat phase, followed by a conventional KT roughening transition. In the unreconstructed case, quite interestingly, they also find two transitions: a non-Ising critical one leading to a "sublattice disordered" flat phase, followed again by a KT roughening.[11]

The model we present in this paper is probably the simplest generalization of the BCSOS model which is able to describe a missing-row (2×1) reconstructed phase as well as the unreconstructed one. It essentially consists of a BCSOS model in which the sign of the, say, x coupling can have either sign—the negative sign favoring the occurrence of reconstruction—and a further neighbor interaction in the x direction is added in order to stabilize the reconstructed case against faceting into a (111) surface. The model is indeed quite similar to the one introduced by Mazzeo *et al.*, except for the choice of the non-nearest-neighbor stabilizing interaction. It has the virtue of being easy to map into a one-dimensional quantum spin-$\frac{1}{2}$ model of the Heisenberg type with further neighbor $S_i^z S_j^z$ interactions. Such a mapping provides a quite powerful way of investigating the full phase diagram of the model, without having to resort to Monte Carlo simulations. Moreover, the insight gained by relating our problem to the large body of knowledge in the field of one-dimensional quantum systems will appear quite evidently.

One of the motivations of our work was a deeper understanding of the nature of the disordered flat phase occurring in this kind of simple modifications of the BCSOS model. In this respect, our study was greatly inspired by the work of den Nijs and Rommelse, in particular by their discussion on the many similarities between the physics of the spin-1 and spin-$\frac{1}{2}$ chain.[14] Within our simple model, we explicitly demonstrate that, indeed, a spin-$\frac{1}{2}$ dimer phase is a natural candidate to represent the disordered flat phase of a fcc(110) surface. From a surface science viewpoint, a better understanding of the phase diagram and of the nature of the disordered flat phases of these surfaces should help in building future experiments directed at their study.

Our results are summarized by the two phase diagrams of Figs. 1 and 2, pertaining to the spin and to the SOS model, respectively. We find four phases in the phase diagram: two ordered phases in which the spins have Néel-type (1×1) and (2×1) long-range order (an unreconstructed and a missing-row reconstructed phase, in the surface language), a spin-liquid phase (representing a rough surface), and an intermediate dimer phase which breaks translational invariance and has a doubly degenerate ground state (a disordered flat surface). The transition from the (2×1) reconstructed phase to the disordered flat phase belongs to the 2D Ising universality class. A critical line with varying exponents separates the unreconstructed phase from the disordered flat phase. Many of the above mentioned features are, we believe, quite robust and should hold for more complicated microscopic models as well. Several scenarios are possible in our phase diagram: First of all, the two-transition scenario for reconstructed surfaces, i.e., Ising deconstruction followed by roughening; next, the possibility—at least in principle—of a first-order transition from a reconstructed to an unreconstructed surface, followed by a preroughening transition to a disordered flat phase, and finally by roughening; finally, for unreconstructed surfaces, either a single roughening transition or two transitions (preroughening followed by roughening), depending on the actual location of the preroughening line, which is highly model dependent.

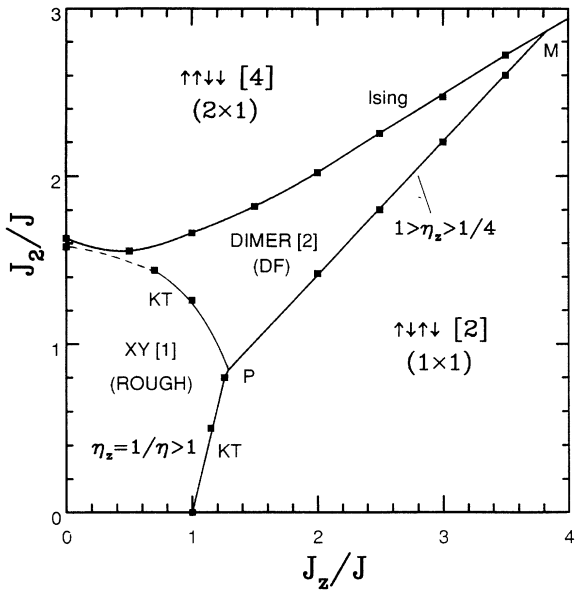

FIG. 1. Ground-state phase diagram for the spin-chain model. PM is a variable exponent (preroughening) line with $1 > \eta_z > 1/4$. Beyond the tricritical point M the character of the line should change to first order. Ground-state degeneracies are given in square brackets. The dashed line indicates the region where strong size effects prevent us from getting accurate data for the exponents.

The rest of the paper is organized as follows. Section II presents the SOS model and its spin-chain counterpart. In Sec. III we describe how the spin-chain phase diagram is obtained. In Sec. IV, finally, we discuss the physics of the disordered flat phase in relationship to the dimer phase of the spin model, and present our conclusions. Relevant technical material on the spin-chain mapping is contained in the Appendix.

II. A SOLID-ON-SOLID MODEL AND ITS SPIN-CHAIN COUNTERPART

The model we want to study is defined on a lattice, schematically shown in Fig. 3, which is comprised of two

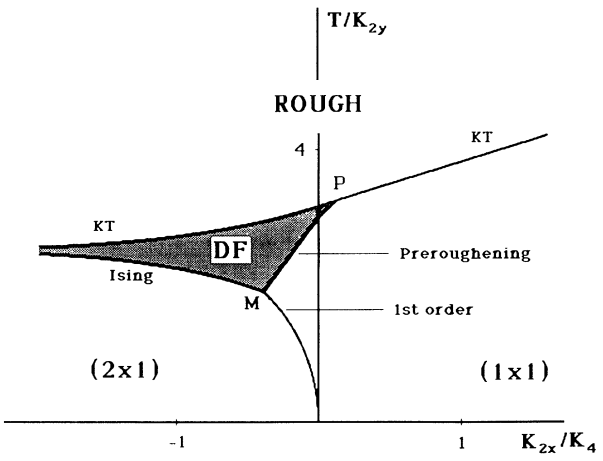

FIG. 2. Ground-state phase diagram for the SOS model as obtained from Fig. 1 using the coupling relationships between the two models. We have taken here $K_4 = 0.1K_{2y}$.

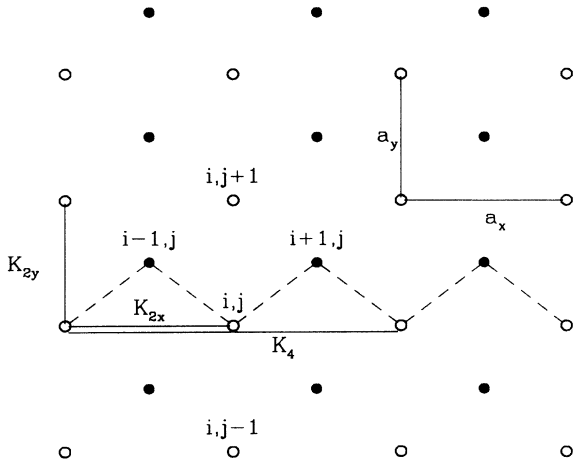

FIG. 3. Schematic top view of the lattice. The site notation (i, j) is explicitly indicated. The white and black sublattices are denoted by open and solid circles, respectively. The dashed line represents the time slice setup for performing the spin-chain mapping. The dimensions (a_x, a_y) of the (1×1) unit cell are shown.

interpenetrating sublattices, conventionally referred to, hereafter, as the white (W) and the black (B) sublattice. In the ideal fcc(110) surface the two sublattices are rectangular, with $a_x = \sqrt{2}a_y$, and one of them sits above the other a distance $a_z = a_y/2$. The notation (i, j) we use for the sites is such that the W and B sublattices are characterized, respectively, by even and odd values of i, whereas the value of j, see Fig. 3, is the same for a horizontal row of W sites and the row of B sites immediately above. To each site of the lattice we associate a height variable $h_{i,j}$ which can take only *integer* values (we fix $a_z = 1$). Moreover, a BCSOS type of constraint is assumed to hold, i.e., the height difference between each site and its nearest neighbors (belonging to the other sublattice) are forced to be ± 1. As a consequence, $h_{i,j}$ are even, say, on the W sublattice and odd on the B sublattice. The Hamiltonian for the model is written as

$$\mathcal{H} = \mathcal{H}_0 + \mathcal{H}_1 ,$$

where $\mathcal{H}_0$ is the BCSOS piece

$$\mathcal{H}_0 = \sum_{i=1}^{N_x} \sum_{j=1}^{N_y} [K_{2y}(h_{i,j} - h_{i,j+1})^2 + K_{2x}(h_{i+1,j} - h_{i-1,j})^2] , \tag{2}$$

describing next-nearest-neighbor interactions with different coupling strengths in the two directions, and

$$\mathcal{H}_1 = \sum_{i=1}^{N_x} \sum_{j=1}^{N_y} K_4 \, (h_{i+2,j} - h_{i-2,j})^2 , \tag{3}$$

(with $K_4 \geq 0$) is a fourth neighbor interaction term in the x direction. Periodic boundary conditions are assumed to hold in both directions. K_{2y} will always be assumed to be *positive* and is generally the largest energy in the problem, since the y direction is the direction of the miss-

ing rows we are trying to describe. The coupling in the x direction, K_{2x}, can instead have either sign as long as $K_4 > 0$ whenever $K_{2x} < 0$, for obvious stability reasons. A negative K_{2x} will quite clearly favor a missing-row type of reconstruction.

The classical $T = 0$ ground states for our model are easy to work out, as a function of the dimensionless ratio $\mathcal{K} = K_{2x}/K_4$. One finds that for $\mathcal{K} > 0$ the ground state is an unreconstructed (1×1) surface, whereas for $-4 < \mathcal{K} < 0$ it is a (2×1) missing-row structure (with missing rows in the y direction), see Fig. 4. For $-8 < \mathcal{K} < -4$ a sequence of larger periodicity $[(3 \times 1), \ldots, (n \times 1), \ldots]$ missing-row phases is obtained, whereas for $\mathcal{K} < -8$ the model no longer describes a (110) surface.

When $K_4 = 0$ and $K_{2x} > 0$, we recover the BCSOS model which can be exactly solved through a mapping to the six-vertex model,[16] and shows a *single transition*, of the Kosterlitz-Thouless type, between a low temperature ordered (unreconstructed) flat phase and a high temperature disordered rough phase.

To proceed further, we map the model in Eqs. (2) and (3) into a one-dimensional quantum spin-$\frac{1}{2}$ Hamiltonian. Details about this mapping are given in the Appendix. It suffices here to say that the gist of the method consists in viewing the y direction as the (imaginary) time direction of an appropriate 1D quantum problem, whose Hamiltonian H_S is selected in such a way that the matrix elements of the imaginary-time evolution operator $e^{-\tau H_S}$ coincide, in the so-called *time-continuum limit*, with the matrix elements of the classical transfer matrix of the original problem.[17] The crucial physical requirement is that the "time" direction must coincide with the hard direction of the classical problem, i.e., the coupling in the y direction has to be much stronger than the other couplings. Anisotropy is not expected to play a role in the phase diagram of the model, and is, moreover, physically quite appropriate in the present case. The nearest-neighbor height constraint suggests that the relevant degrees of freedom can be described by introducing a spin-$\frac{1}{2}$ Hilbert space, and mapping the height difference between nearest neighbors within the same "time slice"—the dashed line in Fig. 3—to the z component of the usual spin operator

$$S_i^z \longleftrightarrow \tfrac{1}{2}(h_{i+1,0} - h_{i,0}) \,. \tag{4}$$

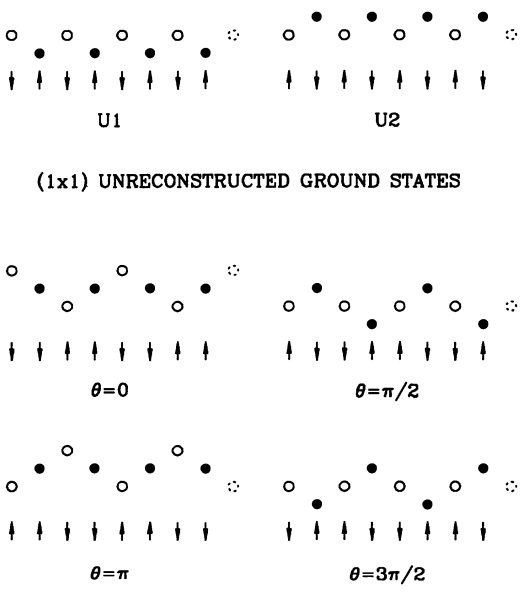

FIG. 4. Schematic height profiles, along a time slice of Fig. 3, of the two ground states of the unreconstructed surface, and of the four missing-row ground states with their clock label. The corresponding spin configurations are explicitly indicated.

Figure 4 illustrates explicitly the mapping of the (1×1) and (2×1) ground states in terms of spin configurations along a time slice. In terms of spin operators, the quantum Hamiltonian reads

$$H_S = -\frac{J}{2}\sum_{i=1}^{N_x}[S_i^+ S_{i-1}^- + S_i^- S_{i-1}^+] + \sum_{i=1}^{N_x}\left(J_z S_i^z S_{i-1}^z + J_2 S_i^z S_{i-2}^z + \frac{J_2}{2} S_i^z S_{i-3}^z\right) , \tag{5}$$

where the spin couplings are related to the original couplings as follows:

$$\begin{aligned} J &= 2\exp(-4\beta K_{2y}), \\ J_z &= 8\beta(K_{2x} + 3K_4), \\ J_2 &= 16\beta K_4, \end{aligned} \tag{6}$$

and $\beta = 1/k_B T$. Periodic boundary conditions on the heights are inherited by the spin model, and also imply that we need to work in the spin sector with zero total magnetization. It is well known that the mapping is such that the free energy per site of the classical problem is related to the ground-state energy per site of the one-dimensional quantum problem, i.e., $\beta f = \epsilon_{\rm GS}$.[18] The temperature clearly enters through the spin couplings, see Eqs. (6), so that any temperature singularity of the classical free energy can be seen as a ground-state energy singularity for the quantum problem as a function of the couplings J_z/J and J_2/J. Moreover, temperature averages for correlation functions of the classical problem can be likewise rewritten in the form of ground-state averages for the corresponding quantum correlation function.[18] In summary, to obtain information about the temperature phase diagram of the classical model we need to study the *ground state phase diagram* of the spin-chain model.

As it is, the spin model in Eq. (5) has not been previously studied, to our knowledge. A similar model, however, has been discussed in Ref. 19, for instance, and has been the topic of a quite extensive literature. It differs from our model in that the second neighbor coupling is taken to be spin isotropic, and the third neighbor coupling is missing, i.e.,

$$H = -\frac{J}{2}\sum_{i=1}^{N_x}[S_i^+ S_{i-1}^- + S_i^- S_{i-1}^+] + \sum_{i=1}^{N_x}[J_z S_i^z S_{i-1}^z + J_2 \vec{S}_i \cdot \vec{S}_{i-2}] \,. \tag{7}$$

We will see later on that many features of the phase diagram of the model in Eq. (7) are indeed present in the phase diagram of our model too. The only exception is an extra phase appearing in our model for sufficiently large J_2, a phase which corresponds, in the surface language, to an ordered (2×1) missing-row structure.

III. ANALYSIS OF THE QUANTUM SPIN-CHAIN MODEL

We start this section by defining the interesting order parameters and correlation functions that we need to look at in order to determine the phase diagram for our model. A quite direct way of defining an order parameter for the quantum spin-chain case is to consider the "square" of the appropriate "staggered magnetization" $N^{-1}\sum_j e^{i(\pi/p)j} S^z_j$. The result can be trivially cast in terms of the Fourier transform $S^{zz}(k)$ of the spin-spin correlation function (the "structure factor"):

$$P^2_{p\times 1} = \lim_{N\to\infty} \frac{1}{N} \sum_j e^{i(\pi/p)j} \langle S^z_0 S^z_j \rangle = \lim_{N\to\infty} \frac{1}{N} S^{zz}_N(\pi/p) \,, \tag{8}$$

where the average has to be intended as a ground-state average. Clearly, ordered phases will be signalled by a structure factor $S^{zz}_N(k)$ which *diverges linearly* with N—for the appropriate k vector—as the length of the system $N \to \infty$. More specifically, $S^{zz}_N(\pi)$ will diverge for a phase with $\uparrow\downarrow\uparrow\downarrow$ (Néel) long-range order (LRO), a (1×1) unreconstructed phase in the surface language, see Fig. 4. A divergence of $S^{zz}_N(\pi/2)$ will instead indicate $\uparrow\uparrow\downarrow\downarrow$ LRO, i.e., a missing-row (2×1) reconstructed surface, see Fig. 4.

Another quantity one needs to look at, in a SOS model, is the height-height correlation function

$$G(\mathbf{r} - \mathbf{r}') = \langle [h_{\mathbf{r}} - h_{\mathbf{r}'}]^2 \rangle \,, \tag{9}$$

which distinguishes a *flat* $[G(r) < \text{const as } r \to \infty]$ from a *rough* $[G(r) \approx \ln(r) \text{ as } r \to \infty]$ phase. The height-height correlation function has a simple translation in the spin-chain model. Restricting our consideration to correlations within the same horizontal row, say $j = 0$, we have

$$\begin{aligned} G(n) &= \langle [h_{n,0} - h_{0,0}]^2 \rangle \\ &= 4 \sum_{i,j=0}^{n-1} \langle GS | S^z_i S^z_j | GS \rangle \\ &= n + 8 \sum_{i=1}^{n} (n-i) \langle GS | S^z_0 S^z_i | GS \rangle \,, \end{aligned} \tag{10}$$

where the last equality follows from assuming translational invariance for the spin-spin correlation function. Notice, in passing, that the term linear in n is exactly cancelled by working at zero total magnetization since, in that case,

$$\sum_{i\neq 0} \langle GS | S^z_0 S^z_i | GS \rangle = -\langle GS | S^z_0 S^z_0 | GS \rangle = -\tfrac{1}{4} \,.$$

Moreover, it is easily checked that whenever the spin-spin correlation function $\langle S^z_0 S^z_n \rangle$ possesses a large distance uniform term of the type $-K/(2\pi^2 n^2)$, $G(n)$ will diverge *logarithmically* as

$$G(n) = \frac{4K}{\pi^2} \ln(n) + \cdots, \quad n \to \infty \,, \tag{11}$$

signalling a rough phase.

We now discuss the information that one can get on different regions of the phase diagram from analytical approaches. In the limit $J_z/J \to \infty$ and $J_2/J \to \infty$ things are very easy to work out. Setting $J = 0$, one finds that for $J_2 < (2/3)J_z$ the Néel states $|\uparrow\downarrow\uparrow\downarrow\cdots\rangle$ and $|\downarrow\uparrow\downarrow\uparrow\cdots\rangle$ are the two possible ground states, whereas for $J_2 > (2/3)J_z$ there are four possible ground states

$$\begin{aligned} |1\rangle &= |\uparrow\uparrow\downarrow\downarrow\uparrow\uparrow\downarrow\downarrow\cdots\rangle, \\ |2\rangle &= |\downarrow\uparrow\uparrow\downarrow\downarrow\uparrow\uparrow\downarrow\cdots\rangle, \\ |3\rangle &= |\downarrow\downarrow\uparrow\uparrow\downarrow\downarrow\uparrow\uparrow\cdots\rangle, \\ |4\rangle &= |\uparrow\downarrow\downarrow\uparrow\uparrow\downarrow\downarrow\uparrow\cdots\rangle \,. \end{aligned} \tag{12}$$

Such a fourfold degeneracy of the ground state reflects the fourfold degeneracy of the (2×1) missing-row surface, as illustrated in Fig. 4.

We now turn to the region of the phase diagram close to $J_z = J_2 = 0$. Clearly, when $J_2 = 0$ (i.e., $K_4 = 0$) the problem reduces to the XXZ Heisenberg chain—the quantum spin-chain counterpart of the BCSOS model—whose physics is well known. For $|J_z/J| \leq 1$ the model is gapless and critical, i.e., the ground-state spin-spin correlation functions decay algebraically at large distances,[19,20]

$$\begin{aligned} \langle S^z_0 S^z_n \rangle &\approx \cos(\pi n) \frac{A}{n^{\eta_z}} - \frac{K}{2\pi^2 n^2} + \cdots, \\ \langle S^+_0 S^-_n \rangle &\approx \cos(\pi n) \frac{B}{n^{\eta}} + \cdots \,. \end{aligned} \tag{13}$$

The exponents η and η_z are exactly known:

$$\eta = \frac{1}{\eta_z} = \frac{1}{\pi} \arccos(-J_z/J) \,. \tag{14}$$

From the previous discussion—see Eq. (11)—it follows immediately that such a phase represents a *rough surface*. For $J_z/J > 1$ the model has a gap and a Néel order parameter, and represents the already mentioned unreconstructed (1×1) phase (the BCSOS flat phase). The transition at $J_z/J = 1$ is of the KT type (the BCSOS roughening transition). Consider now the case $J_2 > 0$. By applying a Wigner-Jordan transformation we can equivalently rewrite our spin model in terms of a spinless fermion model

$$H_F = -J \sum_k^{BZ} \cos(k)\, c^\dagger_k c_k + \frac{1}{N} \sum_q^{BZ} V(q) \rho(q) \rho(-q) \,, \tag{15}$$

where $\rho(q) = \sum_k c^\dagger_k c_{k+q}$ is the density operator and $V(q) = J_z \cos(q) + J_2 \cos(2q) + (J_2/2)\cos(3q)$ is the interaction potential.[21] Zero total magnetization for the

spin model implies a half-filled band for the fermion model. Applying standard techniques in the theory of 1D fermionic systems, i.e., linearizing the band around the two Fermi points at $k_F = \pm\pi/2$ and keeping only interaction processes around the Fermi points, we can write down an effective continuum field theory ("g-ology model").[22] Let $a_{\pm,k}$ be the destruction operator for right-moving (+) and left-moving (−) fermions around the two Fermi points, and let $\rho_\pm(q)$ be the corresponding density operators. The g-ology model reads:

$$H_{\rm eff} = v_F \sum_k k[a^\dagger_{+,k}a_{+,k} - a^\dagger_{-,k}a_{-,k}] + \frac{g_4}{L}\sum_q [\rho_+(q)\rho_+(-q) + \rho_-(q)\rho_-(-q)] + \frac{g_2}{L}\sum_q [\rho_+(q)\rho_-(-q)] + \frac{g_3}{L}\sum_q [\rho^{(+)}(q)\rho^{(+)}(-q) + \rho^{(-)}(q)\rho^{(-)}(-q)], \tag{16}$$

where $\rho^{(+)}(q) = \sum_k a^\dagger_{+,k-q}a_{-,k}$ and $\rho^{(-)}(q) = \sum_k a^\dagger_{-,k-q}a_{+,k}$. To lowest order, the couplings turn out to be $g_4 = J_z + \frac{3}{2}J_2$, $g_2 = 4J_z + 2J_2$, and $g_3 = -2J_z + J_2$. The g_3 term describes *umklapp* processes. In absence of g_3, the g_4 and g_2 terms define a spinless fermion Luttinger model which can be exactly solved (at least when the band cutoff is removed and one works with infinite linear bands). Notice that J_2 competes with J_z in determining the sign of the umklapp term coupling constant g_3. This is a quite general condition under which a pre-roughening line, separating two different gapped phases, is obtained. The continuum model coincides, apart from slightly different weak coupling values for g_2, g_4, and g_3, with the corresponding continuum model derived for the Hamiltonian with spin isotropic second neighbor interaction in Eq. (7).[19] The physics of the two models should indeed be the same in the region close to the origin, and we can therefore borrow most of the conclusions of Ref. 19. Summarizing the results of Ref. 19, we can say that there is a whole region of the phase diagram—for sufficiently small J_2 and J_z—in which the model is within the basin of attraction of a spinless Luttinger model, i.e., g_3 scales to zero upon renormalization. In short, borrowing Haldane's terminology,[23] we have a *Luttinger liquid*. As a result, the spin-spin correlation functions will have exactly the same large distance behavior as in Eq. (13), with suitable coupling dependent exponents η_z and η. Moreover, quite generally, $\eta_z = 1/\eta$ and the constant K is related to the exponents, $K = \eta_z/2$.[23] In the presence of the umklapp term ($g_3 \neq 0$), such a Luttinger liquid becomes *unstable* towards phases having a gap in the excitation spectrum whenever the constant K goes to $\frac{1}{2}$ (or $\eta_z \to 1$). Such a transition is predicted to be in the KT universality class. There is nevertheless a whole line of points, inside the gapped phases, on which effectively the coefficient of the umklapp term g_3 is exactly zero. Such a line will consist of critical points in which the model still behaves as a Luttinger liquid with a varying exponent $\eta_z < 1$. The theory of Ref. 19 also predicts the nature of the two gapped phases to which the Luttinger liquid becomes unstable on either side of the "$g_3 = 0$" line. On one side, the already mentioned ↑↓↑↓ Néel phase is found, whereas on the other side a *spontaneously dimerized phase* should occur.[19]

To determine the actual location of the different lines in the phase diagram we need to resort to a numerical study. We have performed a finite-size scaling analysis of exact diagonalization data for chains up to $N = 28$ sites. The location of the KT lines terminating the Luttinger liquid (rough) phase are determined from the size scaling of the gaps as done, for instance, in Ref. 20. More in detail, the finite-size gaps from the ground state to the first excited state in the spin-1 and spin-0 sectors will determine η and η_z, respectively,

$$N[E_N(S=1,k=0) - E_N(S=0,k=0)] = \pi v_s \eta + \cdots ,$$
$$N[E_N(S=0,k=\pi) - E_N(S=0,k=0)] = \pi v_s \eta_z + \cdots , \tag{17}$$

as $N \to \infty$. The sound velocity v_s can be similarly determined by knowing the gap from the ground state to the first excited state of smallest momentum,

$$N[E_N(S=0,k=2\pi/N) - E_N(S=0,k=0)] = 2\pi v_s + \cdots . \tag{18}$$

An independent way of estimating η_z (or K) comes from the $q \to 0$ limit of the structure factor $S^{zz}_N(q)$. In the Luttinger liquid phase we have, for $q \to 0$, $S^{zz}(q) = (K/2\pi)q + o(q)$, and therefore

$$\lim_{N\to\infty} N S^{zz}_N(q = 2\pi/N) = K . \tag{19}$$

(The advantage of the latter relationship is that the sound velocity v_s does not appear at all.) As an illustration, Fig. 5 shows the finite-size results obtained for $v_s\eta$ (a) and v_s (b) along the line at $J_z/J = 1$ for several values of J_2/J. Power law extrapolations of data for $v_s\eta$, $v_s\eta_z$, and v_s yield the results for the exponents summarized in Fig. 6. Quite unambiguously, a transition—at which $\eta_z = 1/\eta = 1$—occurs for $J_2/J \approx 1.2 \div 1.3$. An independent confirmation of such a result comes from the structure factor data shown in Fig. 7 [see Eq. (19)], from which it is quite clear, for instance, that $J_2/J = 1.4$ is already beyond the transition point (the dashed line in Fig. 7, at $K = \eta_z/2 = 1/2$). A similar procedure has allowed us to determine the location of the KT lines in the phase diagram of Fig. 1.

The location of conventional second-order transitions (which are expected to terminate the large J_2 ordered phase) are determined from the "specific heat" $C_v = \partial^2\epsilon_{\rm GS}/\partial J_2^2$. Figure 8 shows C_v for chains up to $N = 28$ sites as a function of J_2 at $J_z/J = 1$. The location of the maximum of C_v quickly saturates to our estimate of the critical value of J_2, $J_2^{(c)} \approx 1.66J$. Plotting C_v at the estimated $J_2^{(c)}$ versus the logarithm of the system size

(see inset of Fig. 8), we conclude that C_v diverges logarithmically, i.e., the critical exponent $\alpha = 0$. In order to calculate another exponent, we consider the structure factor $S^{zz}_N(\pi/2)$. In the ordered (2×1) phase $S^{zz}_N(\pi/2)$ diverges linearly with N. Exactly at the critical point, however, the spin-spin correlation function will decay as a power law at large distances, $\langle S^z_0 S^z_n \rangle \approx \cos(n\pi/2)/n^{\eta'}$. If the power law exponent η' happens to be strictly less than 1, the structure factor will diverge at the critical point as

$$S^{zz}_N(\pi/2) \approx (\text{const})\ N^{1-\eta'} \quad \text{at } J_2^{(c)} \text{ as } N \to \infty. \tag{20}$$

Figure 9 shows a log-log plot of $S^{zz}_N(\pi/2)$ versus N for $J_z = J$ and different values of J_2 around $J_2^{(c)} \approx 1.66J$. A good straight line fit is obtained only for $J_2 = 1.66J$,

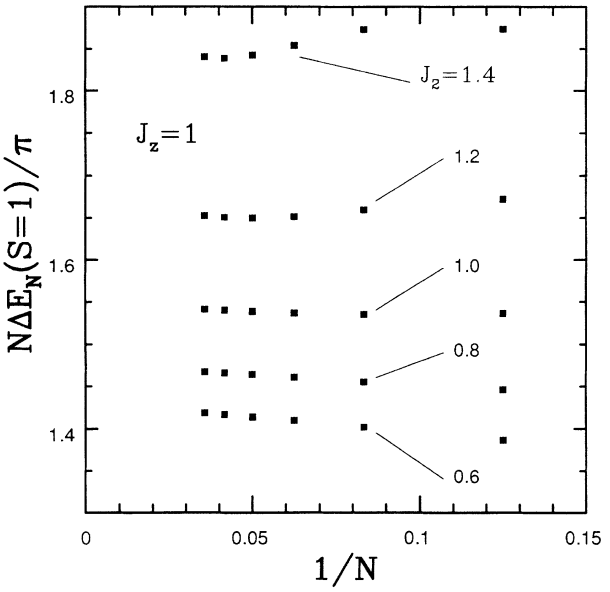

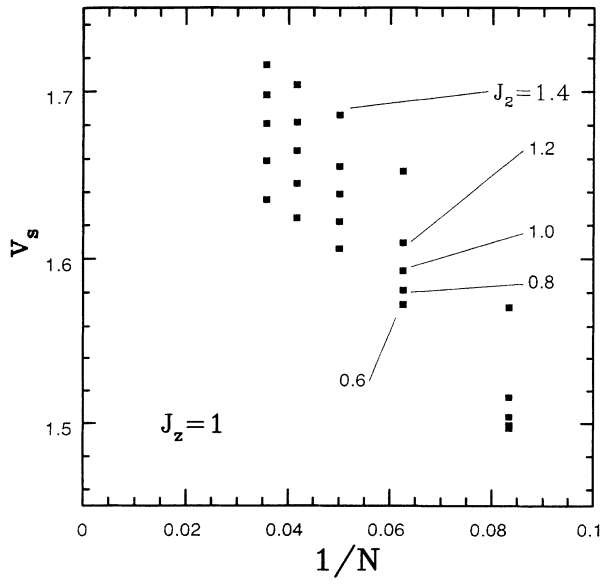

FIG. 5. (a) Size scaling of the gap to the first $S = 1$ excited state. (b) Size scaling of the gap to the first excited state of smallest momentum.

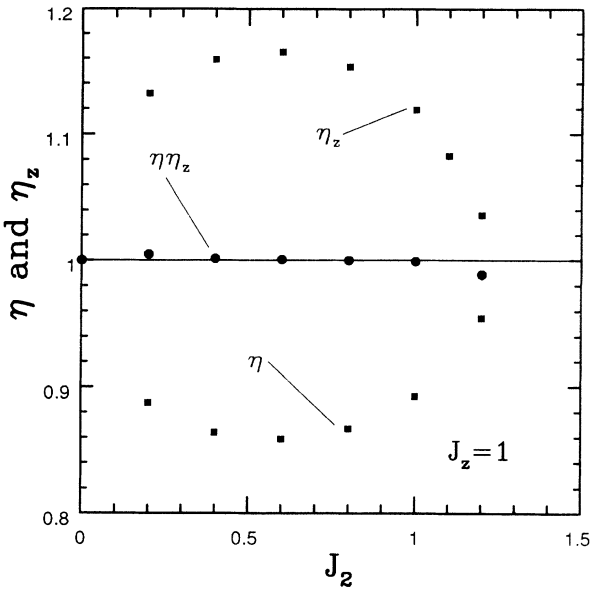

FIG. 6. Summary of the results for the exponent η and η_z along the $J_z = J$ line. A transition, at which $\eta = 1/\eta_z \to 1$, is clearly seen for $J_2/J \approx 1.2 \div 1.3$.

and the slope of the straight line is ≈ 0.75 (the solid line in Fig. 9). This implies $\eta' = \frac{1}{4}$. The transition belongs, therefore, quite unambiguously to the 2D Ising universality class.

As far as the predicted dimer phase is concerned, there are clear numerical indications that we are indeed dealing with a doubly degenerate ground state with a gap above it. Figure 10 shows, for instance, the size dependence of the gap to the first excited $S = 1$ state for $J_2/J = 1.6$ and $J_z/J = 1$. A pronounced increase is seen when one plots $N\Delta E_N$ versus $1/N$, a quite clear hint that ΔE_N is saturating to a constant. On the contrary, the gap to the

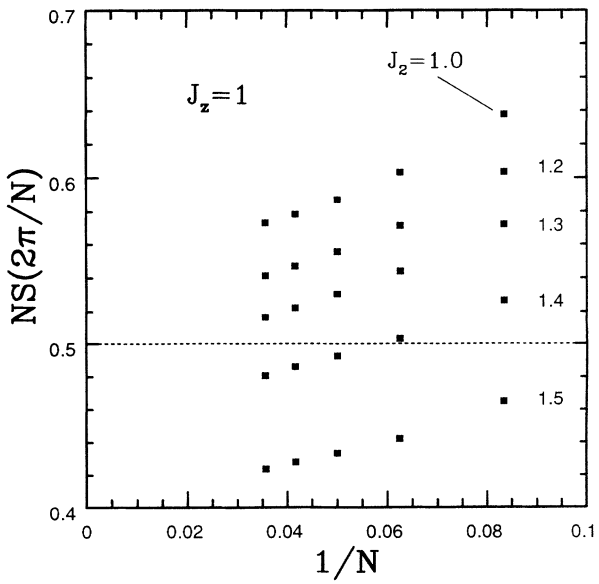

FIG. 7. Size scaling of the $q \to 0$ limit of the structure factor for several values of J_2 along the $J_z = J$ line.

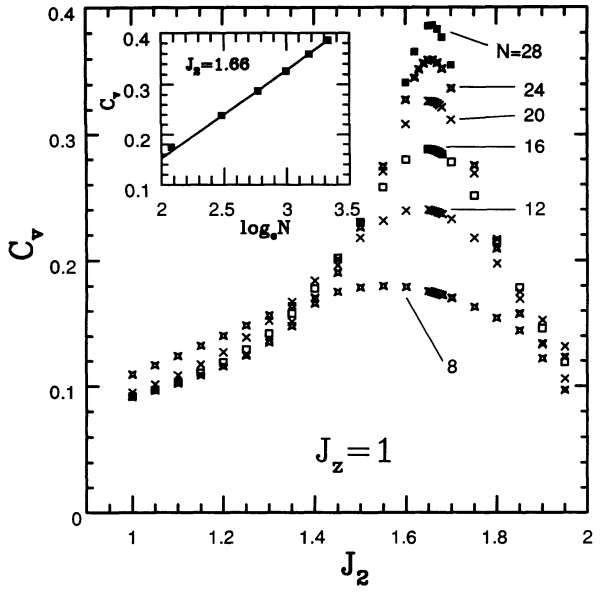

FIG. 8. Size scaling of the "specific heat" $C_v = \partial^2 \epsilon_{GS}/\partial J_2^2$ along the $J_z = J$ line. The peak position saturates at $J_2^{(c)} \approx 1.66J$. The logarithmic nature ($\alpha = 0$) of the divergence of C_v is demonstrated by the inset.

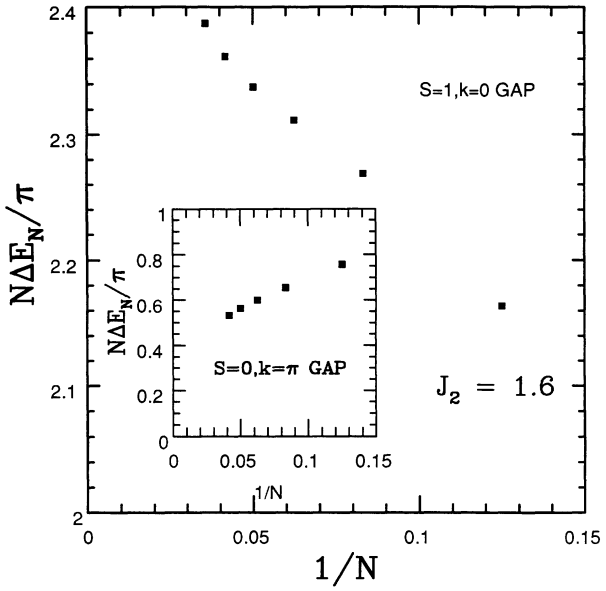

FIG. 10. Size scaling of the gap to the first excited $S = 1$ state in the dimer phase ($J_2/J = 1.6, J_z/J = 1$). The inset shows that the $S = 0$ state of momentum π is degenerate with the ground state for $N \to \infty$.

first excited $S = 0$ state of momentum π is closing up, as shown in the inset of Fig. 10, hinting that such a state is actually degenerate with the ground state in the infinite volume limit. Notice that, with chains of length N up to 28, a reasonably clear gap, such as the one illustrated in Fig. 10 for the $S = 1$ state, is seen only quite far from the transition to the dimer phase. The same argument applies to a direct test of LRO. We have in fact measured a dimer-dimer correlation function

$$D_{ij} = \langle (S^z_{i-1} S^z_i)(S^z_{j-1} S^z_j) \rangle \,, \tag{21}$$

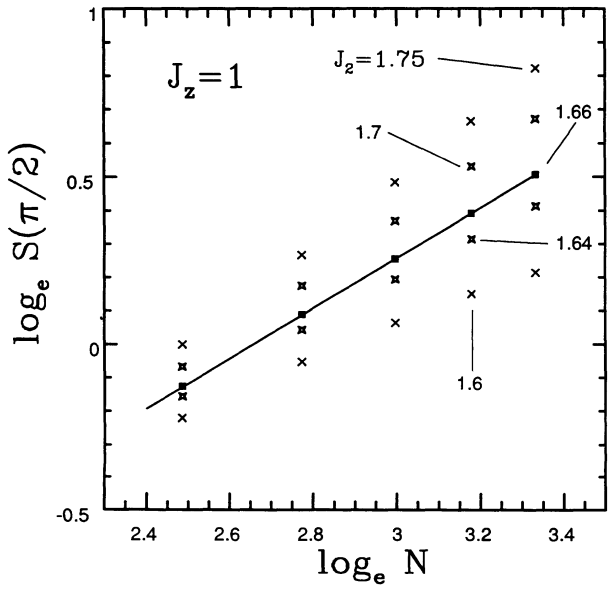

FIG. 9. Size scaling of the $\pi/2$ component of the spin structure factor showing the $N^{3/4}$ divergence at the Ising critical point $J_2^{(c)} \approx 1.66J$.

which is predicted to acquire LRO, $D_{ij} \approx C(-1)^{i-j}$, in the dimer phase. Once again, although a clear tendency to LRO is seen within our "small chains," a full fledged signal of LRO, i.e., the $k = \pi$ structure factor of D_{ij} diverging linearly with N, is almost never seen, except very far from the transition. All these features point in the direction of small gaps and large correlation lengths, which are numerically difficult to assess.

The location of the variable exponent ($g_3 = 0$) line in between the Néel and the dimer phase—characterized by $1/4 < \eta_z < 1$ (Ref. 19)—has been obtained from a combination of the gap scaling procedure in Eq. (17), and from the power law divergence of the structure factor $S^{zz}_N(\pi)$ (using the procedure discussed above for assessing the Ising nature of the second-order transition). The variable exponent line, labeled PM in Figs. 1 and 2, can be identified with the *preroughening* line introduced by den Nijs and Rommelse in the context of restricted SOS models for simple cubic (100) surfaces.[14] The preroughening line merges with the second-order (Ising) line at a tricritical point M, beyond which a first-order line should follow. Such a first-order line should asymptotically tend to approach $J_2 = (2/3)J_z$, the value determined from the $J = 0$ limit.

The final phase diagram for the spin model is depicted in Fig. 1. Most of the lines are quantitative although some points are not determined with great accuracy. The region around the point labeled P shows pronounced size effects which make the exact location of the lines somewhat more uncertain than elsewhere. Even more pronounced size effects are seen in the $J_z \approx 0$ region of the phase diagram where the KT line ending the spin-fluid (Luttinger) phase approaches the Ising deconstruction line. Such large size effects, if on the one hand they prevent us from giving a clear answer to the behavior of the model in that region, are, on the other hand, a quite

probable hint that the Ising and KT lines might merge at some point. We are at present unable to say if the scenario of a single "roughening-induced deconstruction" is indeed at play in our model, and even less able to say if, in such a case, the Ising and KT nature of the original lines would simply be superimposed, as seen in Ref. 9.

A translation of the spin-chain phase diagram in Fig. 1, using the coupling relationships in Eq. (6), allows us to determine the temperature phase diagram for the initial classical SOS model, which is shown in Fig. 2 for $K_4/K_{2y} = 0.1$. The different lines can be obtained, in principle, in a quantitative way from Fig. 1, with discrepancies from the expected exact results which are probably around a few percent, even for not so strongly anisotropic couplings.

IV. THE DIMER PHASE AS A DISORDERED FLAT PHASE

Let us summarize some well known properties of the dimer phase appearing in our phase diagram in Fig. 1, and try to give an interpretation of them in the surface language. (See also Ref. 14.) The dimer phase has a doubly degenerate ground state with a gap above it. Translational invariance is spontaneously broken. All two-spin correlation functions decay exponentially to zero at large distances, which implies—see discussion in Sec. II—that the surface is disordered but flat. There is, however, LRO if one considers four-spin correlation function of the type $\langle(\vec{S}_{i-1}\cdot\vec{S}_i)(\vec{S}_{j-1}\cdot\vec{S}_j)\rangle$. To be more specific, let us consider a representative dimer phase point which corresponds to the exactly solvable case of the model in Eq. (7), i.e., $J_z = J$ and $J_2 = J/2$. This is a particular case of a large class of spin-chain models with competing interactions whose ground state is known to be a simple product of singlets (Madjumar-Gosh models).[24] Explicitly, for any finite- (even) size N there are two ground states (which go into one another by translation of a lattice spacing)

$$|\Psi_1\rangle = |12\rangle|34\rangle\cdots|N-1N\rangle,$$
$$|\Psi_2\rangle = |23\rangle|45\rangle\cdots|N-2N-1\rangle|N1\rangle\,, \qquad (22)$$

where $|ij\rangle = |\uparrow\downarrow - \downarrow\uparrow\rangle/\sqrt{2}$ denotes a singlet between sites i and j. Expanding the product of singlets it is easy to check that each time a pair $\uparrow\uparrow$ appears, it must be followed, sooner or later, by a $\downarrow\downarrow$ pair. The surface is therefore *flat* since a step up is followed necessarily by a step down.

Let us now ask ourselves the following question. Suppose we want to count, in the surface terminology, the difference in the number of white and black local maxima in the surface. For simplicity, we restrict our considerations to sites which are local maxima when considered in the x direction only. In the spin language, a local "maximum" at site j occurs whenever the site $j-1$ has spin $\uparrow$ and the site j has spin $\downarrow$. An operator which "counts" the maximum at j is therefore $(S^z_{j-1} + 1/2)(1/2 - S^z_j)$. The difference between white (even j) and black (odd j) maxima is therefore measured by the order parameter $P_{BW} = (2/N)\sum_j e^{i\pi j}(S^z_{j-1} + 1/2)(1/2 - S^z_j)$. P_{BW} is odd under translation. Its value is 1 on the Néel state $|\uparrow\downarrow\uparrow\downarrow\cdots\rangle$, and -1 on the other Néel state $|\downarrow\uparrow\downarrow\uparrow\cdots\rangle$. (Quite generally, it is different from zero in the whole Néel phase of our phase diagram in Fig. 1.) Consider now the value of P_{BW} on the dimer state $|\Psi_1\rangle$. Using the elementary results that $\langle\Psi_1|S^z_{2j-1}S^z_{2j}|\Psi_1\rangle = -1/4$ and $\langle\Psi_1|S^z_{2j}S^z_{2j+1}|\Psi_1\rangle = 0$, and observing that the terms linear in S^z vanish identically, we arrive at

$$\langle\Psi_1|P_{BW}|\Psi_1\rangle = -\frac{2}{N}\sum_j e^{i\pi j}\langle\Psi_1|S^z_{j-1}S^z_j|\Psi_1\rangle = \frac{1}{4}\,. \qquad (23)$$

(Similarly, $\langle\Psi_2|P_{BW}|\Psi_2\rangle = -1/4$.) We clearly recognize, in Eq. (23), the zz component of the usual dimer order parameter. Therefore a surface interpretation of the dimer order parameter and of the spontaneous breaking of translational symmetry is that either the white or the black sublattice tends to dominate in the surface local maxima. This property has been directly verified by a Monte Carlo simulation of the classical SOS model.[25] More precisely, we have considered an operator $O_{i,j}$ whose value is 1 if the site is an actual 2D local maximum, and zero otherwise, and then constructed the order parameter[25]

$$P^{(\mathrm{surf})}_{BW} = \frac{2}{N_x N_y}\left\langle\sum_{i,j}(-1)^i O_{i,j}\right\rangle\,. \qquad (24)$$

Our Monte Carlo simulation confirms that $P^{(\mathrm{surf})}_{BW} \neq 0$ (in the thermodynamical limit) in the disordered flat phase of Fig. 2.

V. ORDER PARAMETERS AND SURFACE SCATTERING EXPERIMENTS

As exemplified in the preceding section, a disordered flat phase corresponding to the spin dimer phase should be characterized by a spontaneous breaking of the translational invariance, and, consequently, by a predominance of one of the two sublattices in the topmost layer.

These features should be of relevance in the context of surface scattering experiments. We discuss here the case of He scattering. The discussion of the x-ray scattering case can be carried along similar lines, and is dealt with in Ref. 25. In the kinematical approximation, and within a SOS framework, the coherent part of the specular peak intensity with perpendicular momentum transfer in the so-called antiphase configuration is proportional to

$$I^{\mathrm{coh}}(\mathbf{Q} = \mathbf{0}, q_z = \pi/a_z) \propto \left|\left\langle\sum_{i,j} e^{i\pi h_{i,j}}\alpha_{i,j}\right\rangle\right|^2\,, \qquad (25)$$

where $\alpha_{i,j}$ is an appropriate shadowing factor which takes into account the physical requirement that peaks scatter more then valleys.[11,26] For our BCSOS type of model, in which even i's (W sublattice) are associated to even heights $h_{i,j}$ and odd i's (B sublattice) to odd $h_{i,j}$, one immediately concludes that $e^{i\pi h_{i,j}} = (-1)^i$ for any allowed height configuration. $I^{\mathrm{coh}}(\mathbf{Q} = 0, q_z = \pi/a_z)$

would therefore be identically zero if all the atoms were to scatter in the same way [$\alpha_{i,j}=1$ for all (i,j)]. In the assumption that only the local peaks scatter efficiently [$\alpha_{i,j}=1$ if (i,j) is a local peak, $\alpha_{i,j}=0$ otherwise] we obtain that $I^{\rm coh}(\mathbf{Q}=0,q_z=\pi/a_z)$ is proportional to the square of the order parameter introduced above,[12,25]

$$I^{\rm coh}(\mathbf{Q}=\mathbf{0},q_z=\pi/a_z)\propto|P_{BW}^{(\rm surf)}|^2\ . \tag{26}$$

Quite generally, for a reasonably large class of choices of shadowing factors $\alpha_{i,j}$, the breaking of translational invariance should guarantee that $I^{\rm coh}(\mathbf{Q}=\mathbf{0},q_z=\pi/a_z)$ is different from zero (albeit possibly small) in the disordered flat phase considered here. More precisely, this is so for all the shadowing factors which can be written in terms of local operators (in the $h_{i,j}$ variables) whose correlation function is long ranged in the disordered flat phase. We mention here a particularly simple choice of shadowing factors, proposed in Ref. 26, which *does not* involve long-ranged operators: $\alpha_{i,j}=2-n_{i,j}/2$, where $n_{i,j}$ is the number of neighbors of the atom in (i,j) which are found at a level higher than the atom itself. This expression *linearly* interpolates between $\alpha=2$ (local maximum) and $\alpha=0$ (local minimum). It can be recast in the form $\alpha_{i,j}=1-(1/4)\sum_{\rm NN}\Delta h_{i,j}$, where $-\Delta h_{i,j}$ is the height difference between site (i,j) and any of the four nearest neighbor (NN) sites. Indeed, by exploiting this linearity, it is very simple to show that such a choice of α_{ij} leads to an $I^{\rm coh}(\mathbf{Q}=0,q_z=\pi/a_z)$ which is proportional to the square of the (1×1) order parameter $P_{(1\times1)}$ [see Eq. (1)],

$$I^{\rm coh}(\mathbf{Q}=\mathbf{0},q_z=\pi/a_z)\propto\left|\left\langle\sum_{i,j}(-1)^i h_{i,j}\right\rangle\right|^2\ , \tag{27}$$

and therefore vanishes at and beyond the preroughening line.

In conclusion, we have proposed a simple microscopic SOS model for fcc(110) surfaces which can be easily mapped into a spin-$\frac{1}{2}$ quantum chain of the Heisenberg type with competing $S_i^zS_j^z$ interactions. The resulting phase diagram is quite simple and clear. Apart from the obvious unreconstructed and missing-row reconstructed ordered phases, and the high temperature rough phase, we find a disordered flat phase which shows the physics of the dimer spin phase. The possible experimental relevance of such a state has been discussed.

ACKNOWLEDGMENTS

We are grateful to Alberto Parola, Sandro Sorella, Marco Bernasconi, and Erio Tosatti for many enlightening discussions. This research was supported by the Italian Ministry of University and Scientific Research, the "Istituto Nazionale di Fisica della Materia," and the "Consiglio Nazionale delle Ricerche" under the "Progetto Finalizzato 'Sistemi Informatici e Calcolo Parallelo.'"

APPENDIX: DERIVATION OF THE SPIN MODEL

The general idea behind the mapping of a classical statistical mechanics problem in D dimension into a quantum problem in $D-1$ (space) dimensions is quite old, and it is not necessary to repeat it here.[18] For the problem at hand, the details of the mapping are quite similar to the procedure sketched in Ref. 14 for the spin-1 case. We briefly report them here for the reader's convenience.

The starting point for the mapping to a spin model is a T-matrix formulation for the classical partition function

$$\mathcal{Z}=\sum_{h_{i,j}}e^{-\beta\mathcal{H}}=\sum_{h^{(1)}}\cdots\sum_{h^{(N_y)}}\langle h^{(1)}|\hat{T}|h^{(N_y)}\rangle\cdots \times\langle h^{(3)}|\hat{T}|h^{(2)}\rangle\,\langle h^{(2)}|\hat{T}|h^{(1)}\rangle\ , \tag{A1}$$

where $|h^{(j)}\rangle=\{h_{i,j}:i=1,\cdots,N_x\}$ is the jth *row configuration* (the dashed line in Fig. 3), and $\hat{T}$ is the classical transfer matrix. Periodic boundary conditions have been assumed. It is implicitly assumed that the configurations included in the sum have to respect the BCSOS restriction constraint. Indeed, by exploiting this feature, which implies that $h_{i+1,j}-h_{i,j}=\pm1$, we can associate to any row configuration $|h^{(j)}\rangle$ a state $|j\rangle=|S_1^z,S_2^z,\cdots,S_{N_x}^z\rangle$ in the Hilbert space of a quantum spin-$\frac{1}{2}$ chain (of length N_x) by the relationship

$$S_i^z\longleftrightarrow\tfrac{1}{2}(h_{i+1,j}-h_{i,j})\ . \tag{A2}$$

(In so doing we actually lose information on the absolute height of the surface.) The idea is now to try to reproduce the Boltzmann factors appearing in the matrix elements of the classical transfer matrix $\langle h^{(j+1)}|\hat{T}|h^{(j)}\rangle$ by a suitable quantum operator T_Q in the spin Hilbert space, i.e.,

$$\langle h^{(j+1)}|\hat{T}|h^{(j)}\rangle=\langle j+1|T_Q|j\rangle\ , \tag{A3}$$

where $|j\rangle$ and $|j+1\rangle$ are the spin states corresponding to $|h^{(j)}\rangle$ and $|h^{(j+1)}\rangle$, respectively. For the Hamiltomian in Eqs. (2) and (3), the $\hat{T}$-matrix element reads

$$\langle h^{(j+1)}|\hat{T}|h^{(j)}\rangle=\exp\left(-\sum_{i=1}^{N_x}[K_{2x}(h_{i+1}^{(j)}-h_{i-1}^{(j)})^2 +K_4(h_{i+2}^{(j)}-h_{i-2}^{(j)})^2]\right) \times\exp\left(-K_{2y}\sum_{i=1}^{N_x}(h_i^{(j+1)}-h_i^{(j)})^2\right)\ . \tag{A4}$$

The first exponential contains interaction terms within row j and it is quite simple to rewrite it in terms of exponentials of S^z operators only (see below). On the contrary, the second exponential contains the interaction which couples row j to row $j+1$ and is explicitly off diagonal. It is not hard to show that, given all the height contraints, the spin operator $(S_i^+S_{i-1}^-+S_i^-S_{i-1}^+)$ does exactly the job of transforming the spin configuration

around site i in row j, with $h_i^{(j)}$, into the correct spin configuration of the corresponding site in row $j+1$ with $h_i^{(j+1)} = h_i^{(j)} \pm 2$. Such an operator must therefore be multiplied by $e^{-4K_{2y}}$ if we want to reproduce the correct Boltzmann weight. The (diagonal) situation in which $h_i^{(j+1)} = h_i^{(j)}$ is simply given by the identity operator in the spin space. The only tricky point is that $(S_i^+ S_{i-1}^- + S_i^- S_{i-1}^+)$ *does not commute* with the pieces involving S^z, so that care must be taken in ordering the various terms. One can show that the operator T_Q which does the job correctly is given by

$$\begin{aligned} T_Q &= \cdots T(n+3)T(n) \cdots T(7)T(4)T(1), \\ T(n) &= [1 + e^{-4\beta K_{2y}}(S_n^+ S_{n-1}^- + S_n^- S_{n-1}^+)] \\ &\quad \times e^{-8\beta K_{2x}(S_n^z S_{n-1}^z + 1/4)} \\ &\quad \times e^{-4\beta K_4 (S_{n-2}^z + S_{n-1}^z + S_n^z + S_{n+1}^z)^2}, \end{aligned} \tag{A5}$$

where every $T(n)$ for $n = 1, \ldots, N_x$ is included in the product, which is, however, organized in a cyclic way (i.e., with n increasing by 3 from right to left and taken modulo N_x). This is not yet a very useful relationship, because, as mentioned above, the quantum operators appearing in the above expression do not commute. Our aim is indeed to work in a limit in which all the different factors can be grouped together under a single exponential of the form e^{-H_S}. This is the case in the so-called *time-continuum limit*, defined by the fact that $e^{-4\beta K_{2y}} = J/2$ is small, in which case $1 + (J/2)(\cdots) \approx e^{(J/2)(\cdots)}$, and $|\beta K_{2x}|$ as well as $|\beta K_4|$ are also small, so that one can neglect the commutators coming about in regrouping all the exponentials. The final result can be cast in the form

$$\hat{T} \longleftrightarrow T_Q \approx e^{-H_S} \quad \text{(time-continuum limit)}, \tag{A6}$$

where the spin Hamiltonian H_S is given in Eq. (5). The time-continuum limit is essentially a limit of high anisotropy. Whenever anisotropy is not "relevant," one obtains a temperature phase diagram for the classical problem from studying the ground-state phase diagram of the quantum problem. What is more surprising is that the temperature phase diagram turns out to be quantitatively accurate (within a few percent) even for situations in which the classical system is not so strongly anisotropic. This can be explicitly checked in the 2D Ising case,[18] and in the BCSOS case.

[1] J. C. Campuzano, M. S. Foster, G. Jennings, R. F. Willis, and W. Unertl, Phys. Rev. Lett. **54**, 2684 (1985); J. Sprösser, B. Salanon, and J. Lapujoulade, Europhys. Lett. **16**, 283 (1991); D. Cvetko, A. Lausi, A. Morgante, F. Tommasini, and K. C. Prince, Surf. Sci. **269/270**, 68 (1991), and references therein.

[2] I. K. Robinson, E. Vlieg, and K. Kern, Phys. Rev. Lett. **63**, 2578 (1989); M. Kryzowski and K. Kern (private communication).

[3] K. Kern, in *Phase Transitions in Surface Films 2*, Vol. 267 of *NATO Advanced Study Institute, Series B: Physics*, edited by H. Taub *et al.* (Plenum Press, New York, 1990), p. 269, and references therein.

[4] Y. Cao and E. H. Conrad, Phys. Rev. Lett. **64**, 447 (1990).

[5] M. Garofalo, E. Tosatti, and F. Ercolessi, Surf. Sci. **188**, 321 (1987); A. Trayanov, A. C. Levi, and E. Tosatti, Europhys. Lett. **8**, 657 (1989).

[6] J. Villain and I. Vilfan, Surf. Sci. **199**, 165 (1988).

[7] J. Kohanoff, G. Jug, and E. Tosatti, J. Phys. A **23**, L209 (1990); **23**, 5625 (1990).

[8] I. Vilfan and J. Villain, Surf. Sci. **257**, 368 (1991).

[9] M. den Nijs, Phys. Rev. B **46**, 10 386 (1992).

[10] L. Balents and M. Kardar, Phys. Rev. B **46**, 16 031 (1992).

[11] G. Mazzeo, G. Jug, A. C. Levi, and E. Tosatti, Surf. Sci. **273**, 237 (1992); Europhys. Lett. **22**, 39 (1993).

[12] For a review, see M. Bernasconi and E. Tosatti, Surf. Sci. Rep. **17**, 363 (1993).

[13] M. den Nijs, Phys. Rev. Lett. **64**, 435 (1990).

[14] M. den Nijs and K. Rommelse, Phys. Rev. B **40**, 4709 (1989).

[15] $P_{(1\times1)}$ is denoted by P_{BW} in Ref. 11. We prefer to use the symbol P_{BW} for the order parameter which characterizes the disordered flat phase (see Secs. IV and V).

[16] H. van Beijeren, Phys. Rev. Lett. **38**, 993 (1977)

[17] This kind of mapping is slightly different in spirit from the "fermionic mappings" performed in Refs. 9 and 10. With the exception of a "time-continuum limit," it is essentially exact and one does not need to include in the quantum Hamiltonian extra terms describing the merging of four steps (the "fermions" of a fermionic mapping) at the boundary of finite terraces on the surface. See also Ref. 21.

[18] J. B. Kogut, Rev. Mod. Phys. **51**, 659 (1979).

[19] F. D. M. Haldane, Phys. Rev. B **25**, 4925 (1982).

[20] H. J. Schulz and T. Ziman, Phys. Rev. B **33**, 6545 (1986).

[21] This Wigner-Jordan spinless fermion should not be confused with the fermions introduced in Refs. 9 and 10 (which have a spin and describe steps on the surface), and is just an equivalent way of writing Pauli spin operators. In particular, there is no need in Eq. (15) for fermion nonconserving terms describing "dislocations," as is the case for the "fermionic mappings" of Refs. 9 and 10.

[22] J. Sólyom, Adv. Phys. **28**, 201 (1979).

[23] F. D. M. Haldane, J. Phys. C **14**, 2585 (1981).

[24] For a quite detailed elementary account of such models see, for instance, W. J. Caspers, *Spin Systems* (World Scientific, Singapore, 1989).

[25] M. Vendruscolo, G. Santoro, and E. Tosatti (unpublished).

[26] A. C. Levi, R. Spadacini, and G. E. Tommei, in *The Structure of Surfaces II*, edited by J. F. van der Veen and M. A. Hove (Springer-Verlag, Berlin, 1988), Vol. 11.

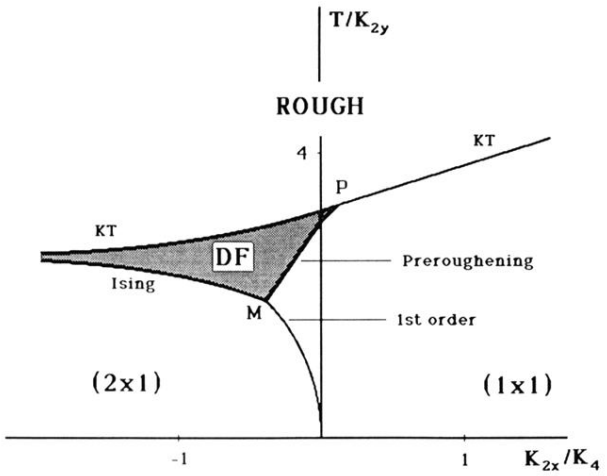

FIG. 2. Ground-state phase diagram for the SOS model as obtained from Fig. 1 using the coupling relationships between the two models. We have taken here $K_4 = 0.1K_{2y}$.